THE JOURNAL OF PHYSICAL CHEMISTRY C

Article

pubs.acs.org/JPCC

Toward Monitoring Electrochemical Reactions with Dual-Wavelength SERS: Characterization of Rhodamine 6G (R6G) Neutral Radical Species and Covalent Tethering of R6G to Silver Nanoparticles

Stephanie Zaleski,[†] M. Fernanda Cardinal,[†] Dhabih V. Chulhai,[∥,▽] Andrew J. Wilson,[⊥] Katherine A. Willets,[⊥] Lasse Jensen,[∥] and Richard P. Van Duyne*[,†,‡,§]

[†]Department of Chemistry, [‡]Department of Biomedical Engineering, and [§]Program in Applied Physics, Northwestern University, 2145 Sheridan Road, Evanston, Illinois 60208, United States

[∥]Department of Chemistry, The Pennsylvania State University, University Park, Pennsylvania 16802, United States

[⊥]Department of Chemistry, Temple University, Philadelphia, Pennsylvania 19122, United States

Supporting Information

ABSTRACT: The combination of electrochemistry (EC) and single molecule surface-enhanced Raman spectroscopy (SMSERS) has recently proven to be a sensitive method to investigate electron transfer (ET) reactions at the single molecule level. SMSERS can both detect single redox-active molecules and potentially monitor both the oxidized (O) and reduced (R) forms of a one-electron ET reaction in a single experiment. Herein, we report progress toward complete monitoring of single ET reactions with EC-SMSERS. We first obtained the solution phase resonance Raman (RR) spectrum of the Rhodamine 6G (R6G) neutral radical (R) with thin-layer resonance Raman spectroelectrochemistry (EC-RRS). The experimental spectrum was then correlated with the spectrum calculated by density functional theory (DFT). We then describe our approach to address the problem of adsorbate (R) loss caused either by desorption or reaction of the neutral radical with trace water or oxygen during the EC-SMSERS experiment. We have investigated a covalent cross-linking reaction which tethers R6G to SERS-active substrates (Ag nanoparticles). Covalently tethered R6G is subsequently characterized by surface cyclic voltammetry (CV) and SERS. Lastly, an optimized cross-linking reaction is devised which enabled the first direct detection of the one-electron reduced form of R6G with SERS. Our findings demonstrate that SERS can simultaneously monitor both O and R of a one-electron ET reaction.

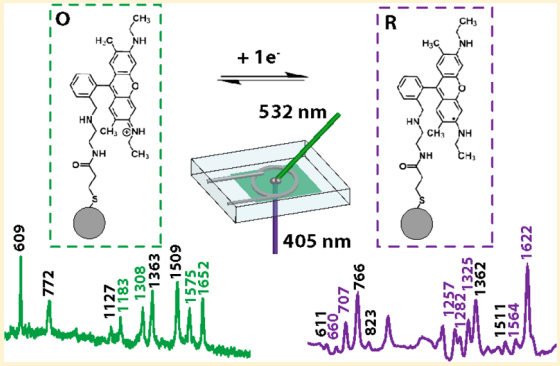

1. INTRODUCTION

The study of electron transfer (ET) reactions has been rapidly moving toward the nanoscale with the aim of understanding fundamental, adsorption site-specific electrochemical behavior. The use of nanoscale electrodes allows for single-molecule detection through redox cycling. However, these nanoscale electrodes are challenging to fabricate reproducibly and amperometric redox cycling methods do not provide structural information about the redox couple being studied.[1−3] Optical techniques such as fluorescence or Raman spectroscopy provide an attractive alternative for studying ET reactions.[4−8] In particular, surface-enhanced Raman spectroscopy (SERS) is a powerful tool to monitor a few to single molecules reacting on a nanoscale electrode, where the loss or gain in SERS signal is correlated to the applied potential and therefore determines the occurrence of an ET event.[9−17] Furthermore, the use of SERS is advantageous since it provides the vibrational spectra of adsorbates, and by comparison of the experimental spectra to theoretically calculated spectra, the electronic and molecular structure changes caused by ET can be determined.

Electrochemical SERS (EC-SERS) and electrochemical tip-enhanced Raman spectroscopy (EC-TERS) have recently been demonstrated as very useful means of studying electrochemistry at the nanoscale.[18] While EC-TERS has the potential to provide direct, correlated structural information on the electrochemically active surface/molecule pair being probed, nonaqueous EC-TERS continues to be quite challenging experimentally due to the open configuration of the scanning probe tip and cell. Therefore, EC-SERS is an excellent means of studying single-electron transfer events in nonaqueous environments. The majority of recent EC-SERS and EC-TERS reports have focused on studying the redox activity of large dye molecules, specifically the phenoxazine dye Nile Blue (NB)[10,11,13,14,17,19−21] and Rhodamine 6G (R6G).[22] The electrochemical and optical activity of NB has been well-characterized: NB undergoes a reversible two-electron, two-proton reduction at pH 2−6 and a two-electron, one-proton

Received: September 6, 2016
Revised: October 12, 2016

DOI: 10.1021/acs.jpcc.6b09022
J. Phys. Chem. C XXXX, XXX, XXX−XXX

Scheme 1. EDC Cross-Linking Reaction[a]

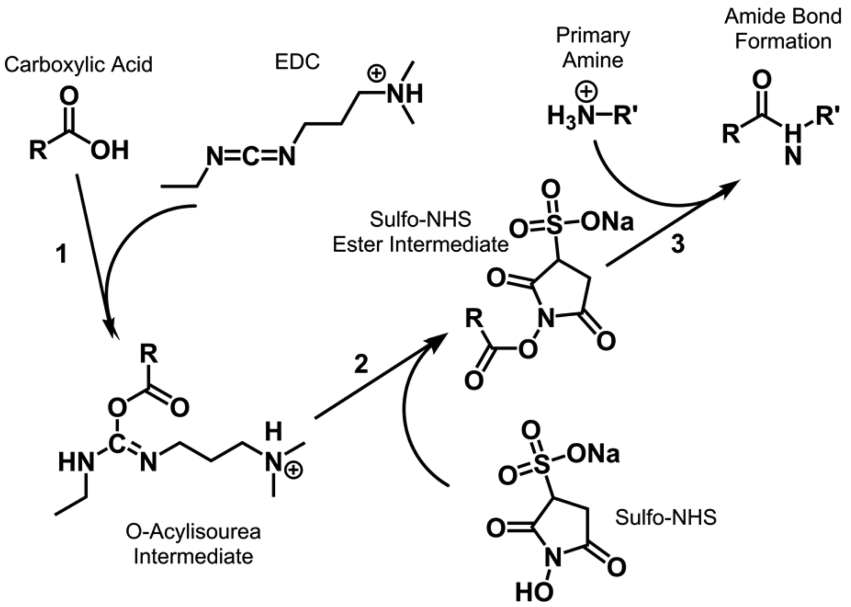

[a]EDC reacts with a carboxylic acid to form an *O*-acylisourea intermediate (1). The primary amine of interest acts as a nucleophile to displace the sulfo-NHS via the sulfo-NHS ester carbonyl group, and form the desired amide bond (2, 3).

reduction at pH 6−10.[19] The oxidized form of Nile Blue (NB_{OX}) absorbs in the visible (~640 nm), while the reduced form (NB_{RED}) absorbs in the near-UV (365 nm).[15] Previous studies monitor the reduction of NB by measuring the loss of the SERS signal for NB_{OX}. On the other hand, R6G undergoes a chemically and electrochemically reversible one-electron reduction in oxygen and water free nonaqueous solution (e.g., acetonitrile). The oxidized form of R6G (the cation) absorbs at 532 nm, and the reduced form (neutral radical) absorbs at 413 nm. Previously, we monitored the loss of R6G cation single molecule SERS (SMSERS) signal excited at 532 nm to indicate electrochemical reduction to its neutral radical form, which can currently only be experimentally realized with EC-SERS. The absorbance and SERS spectra of both redox forms of NB have been reported previously,[15,19] but only the oxidized form of R6G has been characterized with SERS. Full spectroscopic characterization of both redox states of optically active dyes used in EC-SERS experiments can provide a greater insight on the electrochemically induced structural changes and overall site-specific redox activity of these molecules.

The outcome of studying nanoscale electrochemistry with EC-SERS is site-specific molecular electrochemical reactivity of the adsorbate. However, there are experimental challenges that need to be addressed in order to successfully perform EC-SERS and accurately interpret the spectroelectrochemical data. The major experimental challenge for EC-SERS, especially at the single-molecule level, is the loss of SERS signal over the course of successive potential scans. The loss in SERS intensity could originate from desorption, oxygen/water-induced reactive losses,[13,22] and/or potential-dependent alterations in the nanoparticle structure,[23,24] all of which severely limit the number of molecules that can be probed in a single experiment. One strategy to prevent desorptive losses during an EC-SERS measurement is to covalently link the redox probe of interest to the electroactive SERS substrate instead of relying on spontaneous adsorption. Carbodiimide cross-linking forms amide bonds between a primary amine and a carboxylic acid group, and is a common strategy used in forming "zero-length" linkers between two biomolecules.[25] *N*-(3-(Dimethylamino)-propyl)-*N*′-ethylcarbodiimide hydrochloride (EDC) is a common coupling agent for carbodiimide cross-linking, as it is relatively stable and soluble in water. The EDC cross-linking reaction is illustrated in Scheme 1, where the EDC and carboxylic acid form an *O*-acylisourea intermediate (Scheme 1, step 1). That intermediate then reacts with *N*-hydroxysulfo-succinimide sodium salt (sulfo-NHS) to form a sulfo-NHS ester intermediate (Scheme 1, step 2), and the primary amine acts as a nucleophile to displace the sulfo-NHS moiety to form the desired amide bond between the carboxylic acid and the primary amine (Scheme 1, step 3). While the addition of sulfo-NHS is not necessary, it increases the stability of the ester intermediate and improves the overall reaction yield. Recently, the Willets group used EDC cross-linking to tether NB to SERS-active electrodes.[14,20,21] Interestingly, the authors found that the presence of the amide bond and the length of the alkanethiol chain will alter the electrochemistry of NB, as observed with differential pulse voltammetry and high-coverage SERS measurements on Au island films. This finding implies that new molecules or sample preparation strategies for studying nanoscale electrochemistry must be carefully characterized prior to EC-SERS or EC-TERS measurements in order to properly interpret the results.

Herein, we present work toward simultaneous monitoring of both redox states of a one-electron transfer reaction with EC-SERS. First, we characterize the Raman spectrum of the reduced form of R6G (R6G neutral radical, or $R6G^{\bullet}$) with electrochemical resonance Raman spectroscopy (EC-RRS) and correlate the results to theoretical resonance Raman spectra. We then implement EDC cross-linking in order to covalently tether R6G to SERS-active substrates (Ag nanoparticles), and characterize them with cyclic voltammetry (CV) and SERS. For EC-SERS, we study and compare two EDC cross-linking strategies: first, we study a previously reported "heterogeneous" method and we then optimize a novel "homogeneous"

DOI: 10.1021/acs.jpcc.6b09022
J. Phys. Chem. C XXXX, XXX, XXX−XXX

solution-phase cross-linking procedure. Additionally, we compare the SERS and EC-SERS responses of spontaneously adsorbed R6G and EDC-coupled R6G on Ag nanoparticles to ensure that there are no significant spectral differences due to R6G tethering. Finally, we present recent attempts for detecting covalently tethered R6G neutral radical species with 405 nm excitation. This work demonstrates the importance of optimizing the sample preparation for EC-SERS measurements, and presents steps toward the ultimate goal of studying one-electron reactions and simultaneous detection of both redox states of a single R6G molecule with dual-excitation EC-SERS.

2. EXPERIMENTAL DETAILS

2.1. Chemicals. Trisodium citrate dihydrate 90%, silver nitrate +99.99% ($AgNO_3$), sodium chloride +90% (NaCl), tetrabutylammonium perchlorate +99% (TBAP), hydrogen peroxide solution 30% (H_2O_2), ammonium hydroxide solution 28−30% (NH_4OH), (3-mercaptopropyl)trimethoxysilane (MPS), *N*-(2-aminoethyl)rhodamine 6G amide bis-(trifluoroacetate) (R6G-amine), *N*-(3-(dimethylamino)-propyl)-*N*′-ethylcarbodiimide hydrochloride (EDC), *N*-hydroxysulfosuccinimide sodium salt (sulfo-NHS), 2-mercaptopropionic acid (MPA), and 6-mercaptohexanoic acid (MHA) were purchased from Sigma-Aldrich and used without further purification. HPLC grade acetonitrile (MeCN) (≥99.5%) was purchased from Avantor Performance Materials and further purified prior to use by passing through a Pure Process Technology solvent drying system. Milli-Q (MQ) water with a resistivity higher than 18.2 MΩ·cm was used in all preparations.

2.2. R6G Neutral Radical Absorbance Characterization. Thin layer cells were prepared by first using Ag epoxy (Ted Pella) to attach an Ag wire to a cleaned ITO coverslip. Next, a clean glass coverslip was placed on top and the outsides were sealed with TorrSeal epoxy. The cell was clamped together using reverse-close tweezers and allowed to cure overnight. The cell was then placed in a custom-made freeze−pump−thaw (FPT) spectroelectrochemical glass cell with a 1 cm optical path length. A photograph of the cell is shown in Figure S1A. A 1 mM R6G solution was prepared in 100 mM TBAP in acetonitrile. Four FPT cycles were performed on the solution prior to the measurements. Pt wire was used as the counter electrode (CE), and an Ag quasi-reference electrode (QRE) was used. Electrochemical potential was controlled with a CH Instruments Potentiostat (CHI660D) and resonance Raman spectra were acquired.

2.3. SERS Sample Preparation I: Heterogeneous EDC Cross-Linking on Ag Colloids Prefunctionalized on ITO. Ag nanoparticles (AgNPs) were prepared using the Lee and Meisel method.[26] A 2 mL volume of the as-prepared Ag colloids was washed and concentrated by two centrifugation steps (2000 rpm, 6 min; supernatant to 5000 rpm, 6 min), the pellets were redispersed with 0.5 mL of ultrapure water, and to induce nanoparticle aggregation, 0.5 mL of 40 mM NaCl was added. ITO coverslips (22 × 22 mm^2, 8−12 Ω, with copper busbar, SPI Supplies) were cleaned by sonication in isopropanol for 5 min; then they were base treated in 5:1:1 H_2O:NH_4OH:H_2O_2 at 50 °C for 12 min followed by water and isopropanol rinsing steps, to activate hydroxyl groups. Then, ITO coverslips were functionalized with MPS, where the ITO coverslips were incubated in 0.5 mL of MPS in 50 mL of isopropanol for 6 min at room temperature, and then thoroughly rinsed with isopropanol and dried under N_2. Once dried, 0.15 mL of aggregated Ag colloids was immediately drop-cast on the MPS-functionalized ITO and allowed to dry in a N_2 box, after which they were thoroughly rinsed with ultrapure water and dried under N_2. Each clean AgNP-functionalized ITO was immersed in a 10 mM ethanolic solution of MPA or MHA overnight. The sample was then rinsed thoroughly with ethanol and dried with a stream of N_2. Next, 200 μL of 20 mM EDC and 40 mM sulfo-NHS in water was drop-cast on the ITO surface and allowed to react for 30 min in ambient conditions. The sample was then rinsed thoroughly with water and dried with a stream of N_2. Last, 200 μL of R6G-amine in pH 5 phosphate buffer was drop-cast on the surface, allowed to react for 2 h at ambient conditions, rinsed with water and isopropanol, and dried with N_2.

2.4. SERS Sample Preparation II: Homogeneous EDC Cross-Linking on Ag Colloids in Solution. A 5 mL volume of the as-prepared Ag Lee and Meisel colloids were washed and concentrated by two centrifugation steps (2000 rpm, 7 min; supernatant to 5000 rpm, 7 min), and the pellets were resuspended in 0.9 mL of MQ H_2O. Then 20−90 μL of 1 or 10 mM ethanolic solution of mercaptopropionic acid (MPA) or mercaptohexanoic acid (MHA) was slowly and dropwise added to the AgNP solution while vortexing the sample. The AgNP samples were then sonicated for 20 min and centrifuged to remove MPA or MHA excess. The particles were resuspended in 0.45 mL of MQ H_2O under sonication—it is worth noting that they visually appeared aggregated. Then two different methods were used to covalently attach R6G to the AgNP sample:

Method II-A. In this method, 50 μL of 20 mM EDC and 40 mM sulfo-NHS aqueous solution and 50 μL of 140 μM R6G-amine in pH 5 phosphate buffer were added simultaneously, sonicated for 30 min, and then allowed to incubate for an additional 30 min without sonication.

Method II-B. To the Ag colloid 50 μL of 20 mM EDC and 40 mM sulfo-NHS aqueous solutions was added and sonicated for 30 min. The sample was then centrifuged (2000 rpm, 5 min) and resuspended in 0.4 mL of MQ H_2O. Later, 50 μL of 140 μM R6G-amine in phosphate buffer (pH 5) was added to the solution and incubated for 2 h. After each method, either A or B, the sample was centrifuged (2000 rpm, 5 min) and resuspended in 0.3 mL of MQ H_2O, and 25 μL of the colloid solution with 50 μL of MQ H_2O was drop-cast on a cleaned ITO surface and allowed to dry in a N_2 box. The sample was then thoroughly rinsed with MQ H_2O, acetone, and ethanol, respectively, and dried with a N_2 stream.

2.5. EC-SERS Sample Preparation. After the functionalized ITO from sample preparation I or II was fully dried with N_2, copper tape was placed on the ITO to allow for electrical contact. The sample was then mounted on the SMSERS glass sample cell using TorrSeal epoxy (Duniway Stockroom Corp., Fremont, CA) and allowed to cure overnight. Next, the cell was placed under vacuum and the supporting electrolyte was transferred in a vacuum in order to remove oxygen and water, which quenches radical species and/or causes R6G degradation. The assembled cell was connected to the custom FPT cell which was then connected to a custom-built high vacuum line (base pressure ∼ 10^{-6} Torr).[22] The FPT cell was filled with 10−15 mL of electrolyte solution prior to FPT and subsequent solvent transfer to the SMSERS cell. After solvent transfer, the SMSERS cell valve was closed and was disconnected from the FPT cell for spectroscopic measurements.

2.6. Film over Nanosphere (FON) Fabrication. Twenty-five millimeter no. 1.5 circular glass coverslips were first cleaned

DOI: 10.1021/acs.jpcc.6b09022
J. Phys. Chem. C XXXX, XXX, XXX−XXX

with piranha solution for 30 min (3:1 H_2SO_4:H_2O_2), rinsed copiously with MQ H_2O, and then treated with 5:1:1 H_2O:H_2O_2:NH_4OH for 45 min to render the surface hydrophilic. The coverslips were stored in MQ H_2O prior to use. Also, 10−12 μL of 300 nm carboxyl latex microspheres (4% w/v, Invitrogen) was drop-cast, homogeneously distributed onto the glass coverslip, and then allowed to dry. After drying, 200 nm Ag was thermally deposited on the FON mask surface at a rate of 2 Å·s^{-1} under vacuum (~5.0 × 10^{-6} Torr) using a custom-built thermal vapor deposition system.

2.7. Electrochemical Measurements. Surface cyclic voltammetry (CV) measurements of EDC coupled R6G on AgNPs on ITO were performed in a capped scintillation vial. Conductive copper tape was attached onto the border of the ITO surface and extended out 10 cm to make electrical contact. The Pt wire counter electrode was shaped into an ~2 cm diameter ring and placed in close proximity to the ITO surface. The reference potential was determined by a nonaqueous Ag wire quasi-reference electrode (QRE) in a 100 mM tetrabutylammonium perchlorate (TBAP) solution in acetonitrile. All electrochemical measurements in this work use this configuration unless otherwise stated. The supporting electrolyte solution was degassed with N_2 for 30 min prior to obtaining electrochemical measurements. Electrochemical measurements were performed using a CH Instruments potentiostat (CHI660D). Background subtraction and R6G surface coverage were calculated using a custom exponential fitting procedure in MATLAB.

2.8. Raman Instrumentation. RRS spectra of R6G$^\bullet$ in the thin layer cell setup were acquired using a macro Raman setup. A 405 nm CW laser (Micro Laser Systems, Inc.) was passed through a cleanup filter (MaxLine laser cleanup filter, Semrock) to clean up the laser line, and focused on the thin layer cell working electrode surface. The scattered light was back-collected and Rayleigh scattering was filtered out with a notch filter (405 nm StopLine single-notch filter, Semrock). The filtered light was then focused onto a 1/2 m imaging spectrograph (PI Acton SP2500i, Princeton Instruments), dispersed with a 500 nm blaze, 1200 grooves/mm grating and focused onto a thermoelectrically cooled CCD detector (Pixis 400BR, Princeton Instruments).

SERS spectra were acquired on an inverted microscope setup (Nikon Eclipse Ti-U) with a 100× oil immersion objective and 0.5 numerical aperture. Nanoparticle aggregates were initially viewed under dark field illumination with a 0.8−0.95 numerical aperture condenser. To illuminate the entire field of view for SMSERS measurements, a 532 nm CW laser (Millenia VIIIs, Spectra Physics) was focused onto the sample using grazing incidence at an angle of 60° relative to the surface normal. Scattered light was collected from SERS active particles, and laser light was filtered (RazorEdge Long Pass 532 nm Filter, Semrock). For acquisition of SERS spectra at 405 nm, a 405 nm CW laser (Micro Laser Systems, Inc.) was passed through a band-pass filter (MaxLine laser cleanup filter, Semrock) to clean up the laser line, directed to the microscope objective using a 405 nm dichroic beamsplitter (405 nm laser BrightLine single-edge super-resolution laser dichroic beamsplitter, Semrock), and focused on the sample surface using the 100× objective. Scattering was back-collected through the microscope objective, and laser light was filtered (405 nmStopLine single-notch filter, Semrock). Scattered light for both 532 and 405 nm measurements was then focused onto a 1/3 m imaging spectrograph (SP2300, Princeton Instruments, dispersed (1200 grooves/mm grating, 500 nm blaze) and focused onto a liquid nitrogen cooled CCD detector (Spec10:400BR, Princeton Instruments).

2.9. Computational Details. The optimized geometry and normal modes of both R6G$^+$ and R6G$^\bullet$ were obtained with the B3LYP/6-311G* level of theory using NWChem.[27] Vibrational frequencies were scaled by a factor of 0.98 to account for missing anharmonicity in the simulations. The resonance Raman scattering (RRS) of these molecules was simulated using a time-dependent wave packet formalism, where the RRS of R6G$^+$ has been outlined previously.[28] For R6G$^\bullet$, Franck−Condon factors and the transition dipole derivatives (needed for the Herzberg−Teller contributions to the RRS) were obtained from three-point numerical differentiation of the eight lowest excited state energies and transition dipoles, respectively, along mass-weighted normal mode coordinates. In this level of theory, it is the S6 state at 3.11 eV (399 nm) that contributes the most to the RRS of R6G$^\bullet$. This excitation was shifted to 413 nm to account for solvent effects, and the simulated RRS was obtained with an excitation frequency of 405 nm to remain congruent with the experimental setup. All simulated Raman spectra were broadened by Lorentzians with full width at half-maxima of 10.0 cm^{-1}.

3. RESULTS AND DISCUSSION

3.1. Characterization of the R6G Neutral Radical Species with EC-RRS. We first characterized the R6G neutral radical species (R6G$^\bullet$) using electrochemical resonance Raman scattering (EC-RRS). We note that we could not detect the R6G cation (R6G$^+$) with RRS due to its high fluorescence/quantum yield (0.95).[29] The R6G neutral radical species has an extinction coefficient of 5.1 × 10^4 M^{-1} cm^{-1} and therefore should be detectable with RRS.[30] In order to detect R6G$^\bullet$ with RRS, we performed a thin layer spectroelectrochemical measurement to observe the appearance of the R6G neutral radical RR spectrum. We used 405 nm laser excitation in order to overlap with the R6G neutral radical absorbance maximum previously observed at 413 nm.[22] The spectroelectrochemical glassware used consists of a FPT tube, square glass cuvette, and valve (see Figure S1A). The ITO thin layer cell, Ag QRE, and Pt wire CE are suspended in the glassware and extended to the bottom of the glass cuvette. The thickness of the ITO thin layer cell is approximately 300 μm, allowing for any solution in the bottom of the cuvette to be drawn up via capillary action, as illustrated in the schematic in Figure S1B. The potential of the ITO thin layer working electrode is held at −1.2 V (vs Ag QRE) to fully reduce R6G$^+$ to R6G$^\bullet$, and the laser is focused on the ITO in order to acquire RRS spectra. Figure 1 shows that the R6G$^\bullet$ RRS spectrum (red trace) has excellent agreement with its theoretically predicted spectrum (blue trace); peak values for Figure 1 are reported in Table S1.

There are distinctive peak shifts and new modes that appear in the resonance Raman spectrum of R6G$^\bullet$. These spectral shifts will be useful to differentiate between the spectra of R6G$^\bullet$ and R6G$^+$ in an EC-SERS measurement. New modes appear in the R6G$^\bullet$ spectrum centered at 660, 1257, and 1282 cm^{-1}. Modes centered at 1196, 1325, 1564, and 1622 cm^{-1} are shifted significantly (>10 cm^{-1}) in the R6G$^\bullet$ spectrum relative to the R6G$^+$ spectrum. The mode at 660 cm^{-1} is mainly localized on the pendant phenyl ring, as shown in the R6G$^\bullet$ eigenvector diagrams in Figure S2. We also note that position of the pendant phenyl ring in the lowest energy configuration of the R6G$^\bullet$ is slightly rotated with respect to the xanthene ring in

DOI: 10.1021/acs.jpcc.6b09022
J. Phys. Chem. C XXXX, XXX, XXX−XXX

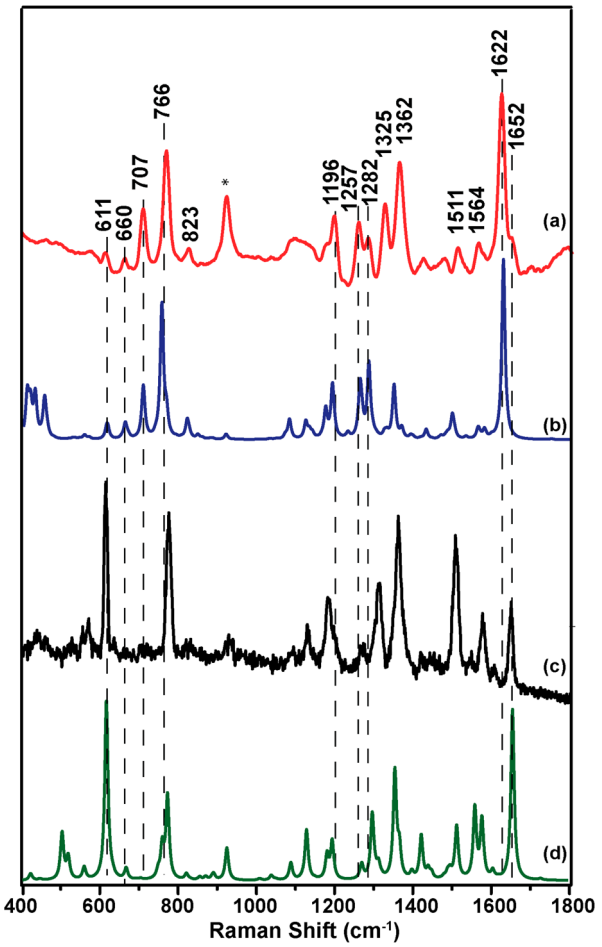

Figure 1. Comparison of experimental and theoretical R6G$^{\bullet}$ and R6G^{+} Raman spectra. (a) Experimental RRS spectrum of 1 mM R6G$^{\bullet}$ in 100 mM TBAP in MeCN, which was acquired in an ITO thin layer cell with an applied potential of −1.2 V (vs Ag QRE). Acquisition parameters: λ_{ex} = 405 nm, P_{ex} = 2 mW, t_{acq} = 120 s (red trace). (b) DFT RRS spectrum of R6G$^{\bullet}$ (blue trace). (c) Experimental SERS spectrum of R6G^{+} acquired from a single AgNP aggregate. λ_{ex} = 532 nm, P_{ex} = 25 mW (grazing incidence), t_{acq} = 5 s (black trace). (d) DFT RRS spectrum of R6G^{+} (green trace).

comparison to the configuration of R6G^{+}, which is most likely the origin of the new 660 cm^{-1} mode. Furthermore, upon reduction of the R6G^{+}, the xanthene ring loses conjugation and, therefore, vibrational modes dominated by the xanthene ring are expected to shift. The most significant shift is the 30 cm^{-1} blue shift from 1652 cm^{-1} (R6G^{+}) to 1622 cm^{-1} (R6G$^{\bullet}$); this mode has been previously calculated to have 89% xanthene character in R6G^{+}.[31] The 1196 cm^{-1} mode is also high in xanthene ring character, which red shifts 16 cm^{-1} compared to the same R6G^{+} mode. Additionally, the loss of the peaks at 925 and 1129 cm^{-1} (40 and 28% xanthene character, respectively)[31] in the R6G$^{\bullet}$ spectrum compared to the R6G^{+} spectrum can also be due to the loss in conjugation of the xanthene ring. Interestingly, the shift in the R6G$^{\bullet}$ 1564 cm^{-1} mode, primarily ethylamine in character, is attributed to a change in symmetry of the vibrational mode (see Figures S2 and S3 and Table S1).

In conclusion, we have successfully characterized the neutral radical species of R6G with EC-RRS and compared our results to theoretically predicted spectra with excellent agreement. There are unique vibrational modes that are present in R6G$^{\bullet}$, making it readily differentiable from its oxidized R6G^{+} form by Raman spectroscopy. Unfortunately, our attempts to detect R6G$^{\bullet}$ by EC-SERS starting from physisorbed R6G^{+} have been unsuccessful, which we attribute to desorption of the neutral radical species from the AgNP surface. Therefore, section 3.2 addresses covalent tethering of R6G onto SERS-active surfaces in order to circumvent adsorption differences and potential loss in EC-SERS signal between these two redox forms.

3.2. EDC Cross-Linking of R6G on Ag Nanoparticles for EC-SERS. *3.2.1. Electrochemical Characterization of EDC-Coupled R6G on AgNPs.* EDC cross-linking requires a primary amine and a carboxylic acid to form an amide bond (see Scheme 1). R6G does not have a primary amine or carboxylic acid moiety, so we implemented an R6G analogue, *N*-(2-aminoethyl)rhodamine 6G amide bis(trifluoroacetate), which we will refer to as R6G-amine. R6G-amine has a primary amine on the pendant phenyl ring instead of the ester moiety, making it possible to EDC couple to an electroactive surface functionalized with a carboxylic acid containing molecule (e.g., carboxylic acid terminated alkanethiol, see Scheme S1). Additionally, the structure of R6G-amine is not significantly altered compared to R6G, and we therefore expect the SERS response to be similar to R6G used in previous experiments.

Prior to performing SERS measurements, EDC-coupled R6G AgNPs on ITO were prepared using sample preparation I (see Experimental Details) and electrochemically characterized with CV to ensure R6G-amine exhibited well-behaved surface electrochemistry. We performed surface CVs on samples prepared with and without the final R6G-amine incubation step. Figure 2A shows the resultant CVs, where $E_{p,red}$ = −0.880 V and $E_{p,ox}$ = −0.878 V for the CV corresponding to the R6G addition step. For ease of fitting the cathodic and anodic current peaks, we performed an exponential baseline correction of the CV with EDC cross-linked R6G-amine. The baseline-corrected CV is shown in Figure 2B. The difference in the reduction potentials of the EDC-coupled R6G and previously measured CVs of AgNPs on ITO is most likely due to the presence of thiolated molecules on the AgNP surface, which in turn effects redox potentials.[22] We note that there are no peaks in the sample without R6G (black dashed trace, Figure 2A), simply a background capacitive feature characteristic of surface CVs, indicating the success of the EDC cross-linking reaction. The peak separation of the EDC-coupled R6G surface CV is 2 mV, which strongly indicates a well-behaved, surface-bound species.[32−34] The peak widths of the cathodic and anodic waves

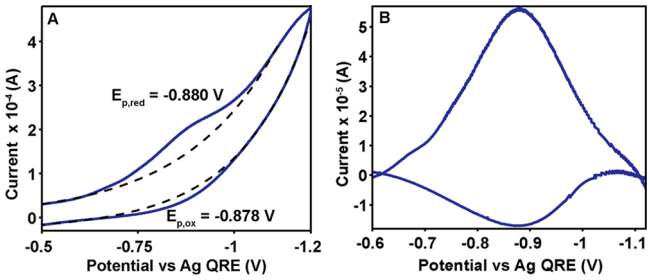

Figure 2. Cyclic voltammetry measurements of EDC-cross-linked R6G-amine on AgNPs on ITO. (A) Thiol, EDC, and sulfo-NHS added to AgNPs with R6G-amine (blue trace) and without R6G-amine (black dashed trace). Scan rate = 100 mV/s. (B) The blue trace in (A) was fit to an exponential and RC-term baseline, which was then subtracted from CV of EDC-cross-linked R6G on AgNPs from (A) to yield the displayed CV.

DOI: 10.1021/acs.jpcc.6b09022
J. Phys. Chem. C XXXX, XXX, XXX−XXX

at half-height are greater than what is expected for a one-electron reaction (~90 mV).[24] This can be attributed to interactions between adjacent R6G molecules tethered to the surface as well as heterogeneities between surface interactions.[35] We then calculated the R6G-amine surface coverage:

$$Q_c = \frac{1}{\nu}\int_{E_0}^{E_\tau} i_c \, dE \quad (1)$$

where Q_c is the cathodic charge, ν is the CV scan rate, E_τ is the final potential, E_0 is the initial potential, and i_c is the cathodic current. Integrating eq 1 yields eq 2:

$$\Gamma_c = \frac{Q_c N_A}{nFA} \quad (2)$$

where Q_c is the cathodic charge, N_A is the Avogadro constant, n is the charge passed in the ET reaction being studied, F is Faraday's constant, and A is the area of the electrode. To calculate the cathodic and anodic charges, we first corrected for the capacitive background in the surface CV. Q_c was determined from the integrated area under the cathodic peak in Figure 2B and was calculated to be 1.29×10^{-4} C; Q_a, or the anodic charge, was calculated to be 3.72×10^{-5} C. The discrepancy between Q_c and Q_a indicates how sensitive the system is to oxygen or water, which can react with the reduced R6G neutral radical species and render the one-electron transfer chemically irreversible. If we approximate the area of the electrode to be 2 cm^2 and $n = 1$, Γ_c is 4.03×10^{14} molecules/cm^2. This value is consistent with previous calculations for determining monolayer surface coverages, where ~10^{14} molecules/cm^2 was the upper limit of monolayer coverage of NB on ITO[15] and 4.64×10^{14} molecules/cm^2 was the high coverage limit of ferrocene-terminated alkanethiol.[35] We note that our calculation is likely to be an overestimation of surface coverage due to the added AgNPs on the ITO surface and therefore higher total surface area of the electrode. The CV measurements confirm that R6G amine is covalently bound to the NP surface and is electrochemically active, and it should be readily observable with SERS.

3.2.2. Heterogeneous EDC Cross-Linking: AgNPs on ITO and AgFONs. After characterizing the electrochemistry of EDC-coupled R6G on AgNPs, we then analyzed samples prepared via sample preparation I with SERS. This was done to ensure that the SERS response of the EDC coupled R6G-amine is not significantly different from that of R6G physisorbed onto AgNPs, as previously used in EC-SMSERS experiments.[22] Figure 3 shows the SERS spectra of R6G-amine heterogeneously EDC-coupled with mercaptopropionic acid (MPA) compared to physisorbed R6G on AgNPs. Table S1 includes the corresponding peak positions for comparison purposes. Most vibrational modes of the EDC cross-linked R6G-amine are in strong agreement with those of physisorbed R6G; however, there are peak shifts in the 1300−1600 cm^{-1} region which we ascribe to the presence of a new amide mode from the EDC cross-linking reaction. Despite the high SERS intensity observed in this reference spectrum, acquiring many high quality SERS spectra from the sample was very challenging due to strong fluorescent backgrounds throughout the sample and low density of SERS-active AgNP aggregates. Additionally, we were not able to acquire SERS spectra from an AgNP sample prepared using mercaptohexanoic acid (MHA, data not shown). Therefore, using this type of sample preparation (heterogeneous EDC cross-linking) to collect a statistically

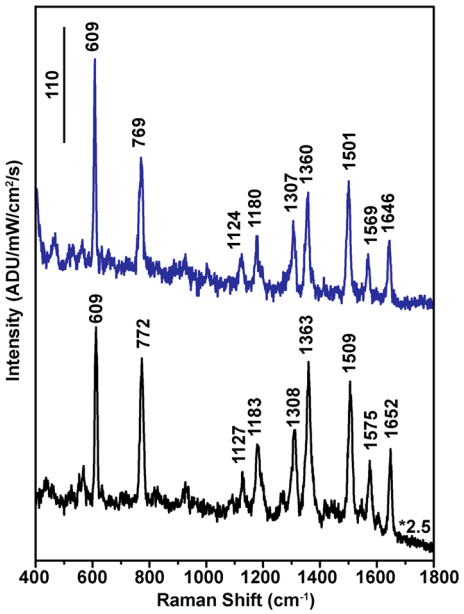

Figure 3. Representative SERS spectra of heterogeneously EDC-cross-linked R6G-amine$^+$ on AgNPs (blue trace) compared to physisorbed R6G$^+$ on AgNPs (black trace). R6G SERS acquisition parameters: λ_{ex} = 532 nm, P_{ex} = 25 mW (grazing incidence), t_{acq} = 5 s. R6G-amine SERS acquisition parameters: λ_{ex} = 532 nm, P_{ex} = 15 mW (grazing incidence), t_{acq} = 3 s.

significant number of SMSERS spectra would be extremely arduous. We attribute the lack of high-quality SERS spectra from samples prepared by sample preparation I to the fact that EDC-coupled R6G-amine molecules are located on SERS hot spots at a low yield since Ag particles were preaggregated prior to deposition on the ITO surface. Additionally, the large fluorescent backgrounds (not shown) could also be due to R6G-amine molecules potentially bound to the ITO surface and away from SERS active sites.

We confirmed that the SERS spectra, as well as fluorescent background, of R6G-amine$^+$ observed originated from the successful linkage of R6G-amine to the Ag surface by performing the same heterogeneous EDC-coupling procedure on an Ag film over nanosphere (AgFON) SERS substrate. FONs are highly enhancing SERS substrates with a high density of hot spots.[36,37] We therefore expect to observe SERS signal if the R6G-amine is bound to the AgFON surface. We performed the EDC cross-linking reaction on an AgFON optimized for 532 nm excitation[36] with both MPA and MHA, and we found that both yield strong SERS signals sitting on top of a fluorescent background, as shown in Figure 4. Because R6G-amine is not directly adsorbed to the AgFON surface, it is possible that the fluorescence background is originating from a surface-enhanced-fluorescence (SEF) effect. Like SERS, SEF is highly distance dependent; fluorescence enhancement reaches a maximum at nanoparticle−molecule distances of ~2−3 nm and is quenched within <1 nm of the enhancing substrate due to nonradiative relaxation to the metal particle.[38,39] In Figure 4, we attribute the pronounced fluorescence backgrounds to SEF and the presence of MHA and MPA acting as spacers between the EDC-cross-linked R6G and the Ag nanoparticle surface. Moreover, the MPA EDC cross-linked R6G-amine SERS signal is approximately 2 times more intense than that of the MHA, which is expected due to the distance dependence of SERS. This result indicates the importance of using a short-chain

DOI: 10.1021/acs.jpcc.6b09022
J. Phys. Chem. C XXXX, XXX, XXX−XXX

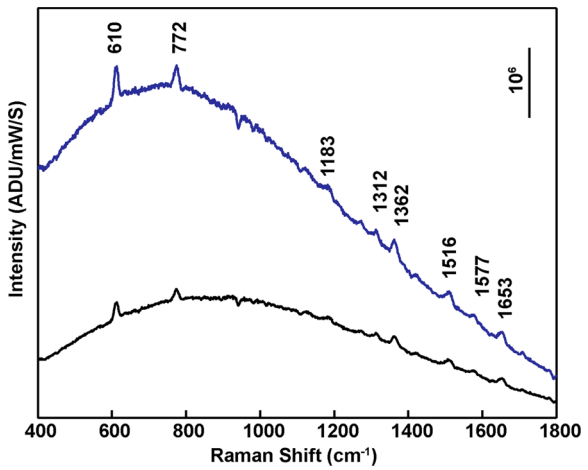

Figure 4. SERS spectra of EDC-coupled R6G-amine$^+$ using MPA (blue trace) and MHA (black trace) on an AgFON substrate. Acquisition parameters: λ_{ex} = 532 nm, P_{ex} = 3 μW (40× objective, epi illumination), t_{acq} = 5 s.

alkanethiol when coupling molecules to the surface in order to obtain the maximum SERS signal, especially for SMSERS studies. Now that we were successfully able to confirm surface-bound R6G-amine on AgFONs with SERS, the current experimental limitations in the framework of performing EC-SMSERS studies led us to develop a novel, optimized EDC cross-linking procedure on AgNPs for EC-(SM)SERS studies.

3.2.3. Homogeneous EDC Cross-Linking of R6G on AgNPs. An alternative sample preparation strategy, which we refer to as homogeneous EDC cross-linking, was developed in order to minimize background fluorescence and to increase the density of SERS-active AgNP aggregates. There are two advantages to the "homogeneous" EDC cross-linking procedure in comparison to the heterogeneous method: first, washing steps performed between each reaction step minimize excess of reactants in solution, and second, the colloids are drop-cast on the ITO after EDC cross-linking, avoiding direct binding of R6G-amine to the ITO and maximizing the R6G-amine molecules located in nanoparticle hot spots. We optimized the homogeneous cross-linking procedure by testing two thiolated acid concentrations and two different EDC reagent/R6G-amine addition steps, as highlighted in Table S2 and Scheme 2. We also investigated the influence of washing steps after carboxylic acid terminated alkanethiol addition in order to evaluate the effect of unreacted reagent excess in solution (S9 and S10 did not have a washing step, see section 2.4, methods II-A and II-B).

For SERS measurements, samples prepared with the MPA thiol and washing steps (S3, S5, and S6, Figure 5 and Table S2) provided the best results. These specific samples resulted in a high density of SERS-active AgNP aggregates on the ITO that had minimal fluorescent background and were stable over time. Sample SERS spectra are shown in Figure 5 and Figure S4, and average 610 cm^{-1} peak intensities are reported in Table S2. The highest average signals were obtained from the samples prepared with 10 mM MPA, which is most likely due to the higher density available sites for EDC reaction to occur, and therefore more R6G EDC cross-linked to the AgNPs. Samples prepared by S5 and S6 (Figure 5ii,iii) were prepared with the same MPA concentration but different timing for R6G-amine addition with respect to EDC reagents, and we observe that the SERS signal intensity is greater for the simultaneous addition of the EDC reagents and R6G-amine. One origin for the difference in average SERS signal intensity between S5 and S6 is that some of the EDC can react with water and is rendered inactive prior to the addition of R6G-amine in method II-B. We observed relatively weaker and less consistent SERS signals from the unwashed MPA sample (S10) as illustrated in Figure S4, which could originate from the EDC reagents reacting with unbound MPA in the solution instead of surface-bound MPA. Interestingly, we were not able to obtain SERS signals from the samples prepared with the MHA thiol, as shown in representative spectra in Figure S4 (S1, S2, S4, S7–S9). We attribute the lack of SERS signal in MHA samples to the distance dependence of SERS and/or insufficient coupling of the R6G-amine on SERS-active hot spots.

Based on our experimental results, we concluded that S6 appeared to be an optimized homogeneous EDC cross-linking procedure, and we performed EC-SERS excited at 532 nm with

Scheme 2. Schematic (Not to Scale) of Homogeneous EDC-Cross-Linking of R6G Performed on AgNPs in Solution

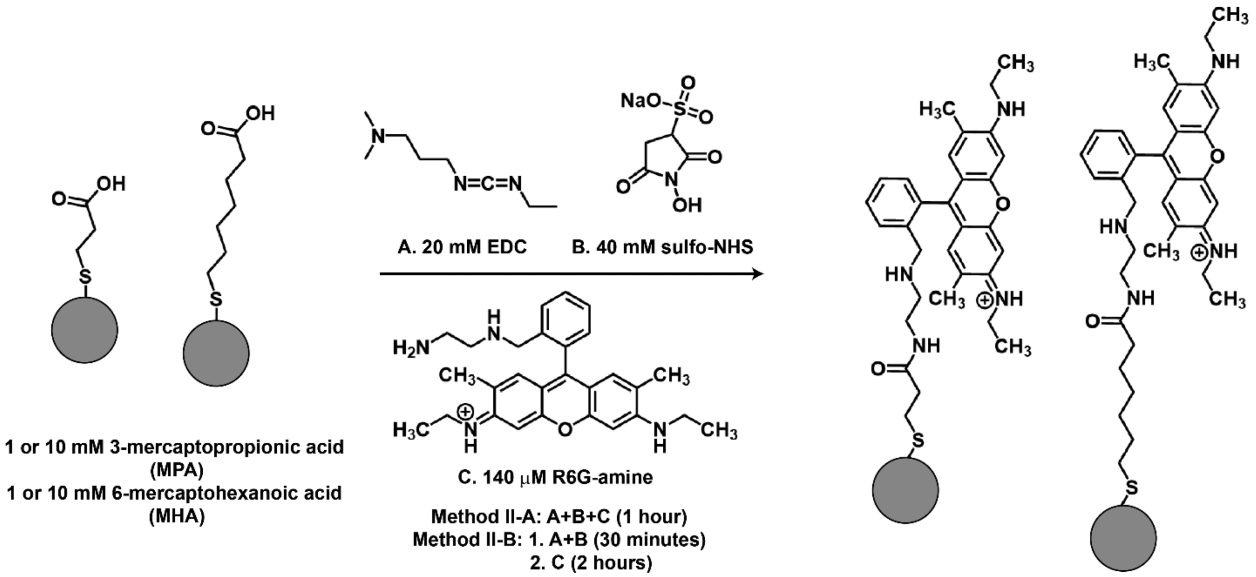

DOI: 10.1021/acs.jpcc.6b09022
J. Phys. Chem. C XXXX, XXX, XXX−XXX

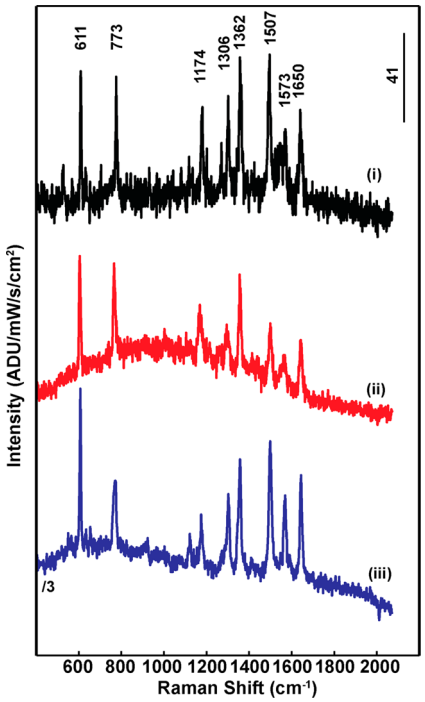

Figure 5. Samples prepared that exhibited stable, reproducible R6G-amine$^+$ SERS signal. (i) Representative SERS spectrum of sample prepared by S3. λ_{ex} = 532 nm, P_{ex} = 12.7 mW (grazing incidence), t_{acq} = 3 s. (ii) Representative SERS spectrum of sample prepared by S5. λ_{ex} = 532 nm, P_{ex} = 12.7 mW (grazing incidence), t_{acq} = 10 s. (iii) Representative SERS spectrum of sample prepared by S6. λ_{ex} = 532 nm, P_{ex} = 15.1 mW (grazing incidence), t_{acq} = 5 s.

samples prepared with the same conditions as S6 (Figure 6). The SERS signal dependence of R6G EDC coupled on a single AgNP aggregate versus applied potential behaved similarly to that of R6G physisorbed on single AgNP aggregates.[22] As shown in Figure 6, the SERS signal is lost at −1.0 V, indicating reduction of R6G-amine$^+$ to R6G-amine$^\bullet$, and returns at −0.7 V, indicating oxidation of R6G-amine$^\bullet$ to R6G-amine$^+$. The R6G-amine$^+$ signal exhibits sharp peak line widths distinctively from known high-coverage R6G EC-SERS spectra,[22] which is indicative of a few to single molecules present per AgNP aggregate.[40] Upon reoxidation of R6G-amine$^\bullet$ to R6G-amine$^+$, we find that the return signal is not as intense as the initial R6G-amine$^+$ signal. Because the R6G-amine molecules are covalently tethered to the surface, it is unlikely the signal loss is from molecular diffusion. The loss in signal intensity more likely originates from potential-induced structural change of the AgNP aggregate or losses due to the presence of trace amounts of oxygen and water, previously observed in EC-SERS studies.[23,24] Since with these measurements we were able to observe EC-SERS behavior excited at 532 nm, comparable to physisorbed R6G on AgNPs, we then attempted to observe the SERS spectrum of the reduced R6G-amine$^\bullet$ species with 405 nm excitation from the same sample. Figure 7 shows representative EC-SERS spectra taken from a single AgNP aggregate at applied potentials of −0.6 and −1.0 V, which is based on the potentials where the cation signal is on and off at 532 nm (Figure 6). The spectrum acquired at −0.6 V illustrates that in the absence of resonance enhancement (405 nm excitation) no spectral features from R6G-amine$^+$ can be detected, whereas the spectrum acquired at −1.0 V presents certain features that can be attributed R6G-amine$^\bullet$. For

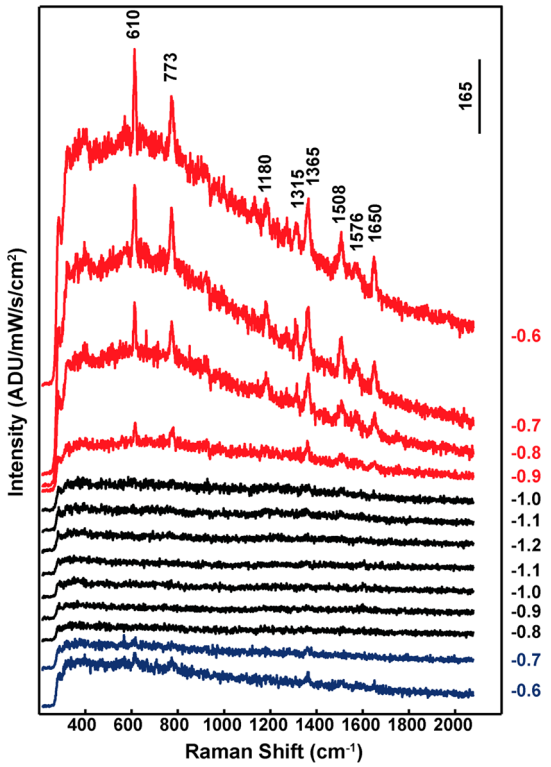

Figure 6. Representative EC-SERS spectra of R6G-amine$^+$ homogeneously EDC-cross-linked onto AgNPs. Samples were prepared by preparation method II-B, S6 (Table S2). The potential is stepped in 0.1 V steps from −0.6 to −1.2 V back to −0.6 V, with the first red spectrum at −0.6 V as the first potential step. R6G-amine$^+$ is fully reduced to R6G-amine$^\bullet$ at −1.0 V (black trace) and is oxidized at −0.7 V (blue trace). R6G-amine SERS acquisition parameters: λ_{ex} = 532 nm, P_{ex} = 15 mW (grazing incidence), t_{acq} = 3 s.

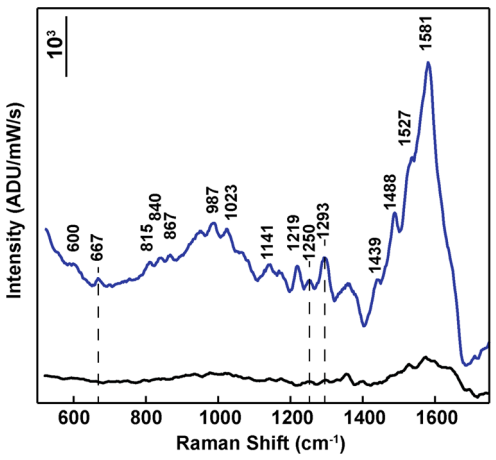

Figure 7. Representative SERS spectra of R6G-amine$^\bullet$. Spectra were acquired at an applied potential of −0.6 V (black trace) and −1.0 V (blue trace). Sample prepared using homogeneous EDC cross-linking procedure (sample preparation S6, Table S2). Dashed lines indicate peaks unique to R6G-amine$^\bullet$. Acquisition parameters: λ_{ex} = 405 nm, 100× objective, P_{ex} = 90 μW (epi illumination), t_{acq} = 2 s.

comparison to theoretical calculations and previous data, the peaks in the 405 nm excitation −1.0 V spectrum are listed in Table S1 (R6G-amine$^\bullet$ column). In particular, we observe the appearance of peaks at 667, 1250, and 1293 cm^{-1} which are in close agreement with the R6G$^\bullet$ experimental RRS peaks at 660,

DOI: 10.1021/acs.jpcc.6b09022
J. Phys. Chem. C XXXX, XXX, XXX−XXX

1257, and 1282 cm^{-1}. Slight discrepancies between the $R6G^{\bullet}$ RRS and R6G-amine$^{\bullet}$ SERS are expected due to the presence of the amide group and the secondary amine on the pendant phenyl ring. Additionally, we observe a broad feature in the 1400−1600 cm^{-1} region, which we do not observe for $R6G^{+}$ with 532 nm excitation; we attribute this broad feature to amorphous carbon background formation. We note that this is the first demonstration of detection of a rhodamine radical species with SERS, and the first demonstration of detecting both redox species of a molecule at few-molecule levels using a dual-wavelength SERS approach. Overall, our results demonstrate the feasibility of monitoring both redox states with EC-SERS.

4. CONCLUSIONS

In this work, we present the spectroscopic characterization of the reduced form of R6G, the R6G neutral radical, and have optimized a new method for preparing SERS-active nanoparticle aggregates using EDC cross-linking. We find that both the electrochemistry and SERS response of the EDC-coupled R6G-amine are not drastically different from those for its physisorbed R6G analogue, and we have successfully optimized a "homogeneous", solution-phase EDC coupling procedure with AgNPs. We then use our optimized EDC coupling procedure to demonstrate the first SERS detection of the R6G neutral radical species using a dual-wavelength SERS approach. The distinct spectral changes between the R6G cation and neutral radical allow for more sensitive monitoring of electrochemical reactions with EC-SERS due to the ability to observe both O and R species simultaneously. Moreover, the work demonstrated herein paves the pathway for future EC-SMSERS experiments, specifically for simultaneous dual-wavelength EC-SMSERS on a single AgNP aggregate.

■ ASSOCIATED CONTENT

Supporting Information

The Supporting Information is available free of charge on the ACS Publications website at DOI: 10.1021/acs.jpcc.6b09022.

Tables with peak position values for $R6G^{+}$ and $R6G^{\bullet}$, eigenvector diagrams of select $R6G^{+}$ and $R6G^{\bullet}$ modes, experimental schematics, photographs of custom glassware for EC-RRS experiments, table summarizing homogeneous EDC sample preparation conditions, and supplementary SERS spectra from different homogeneous EDC sample preparations (PDF)

■ AUTHOR INFORMATION

Corresponding Author

*E-mail: vanduyne@northwestern.edu. Tel.: (847) 491-3516.

Present Address

[▽]D.V.C.: Department of Chemistry, University of Minnesota, 207 Pleasant St. SE, Minneapolis, MN 55455, USA.

Author Contributions

All authors have given approval to the final version of the manuscript.

Notes

The authors declare no competing financial interest.

■ ACKNOWLEDGMENTS

This work was supported by the Air Force Office of Scientific Research MURI (FA9550-14-1-0003) and the National Science Foundation (MRSEC NSF DMR-1121262 and NSF CHE-1506683). S.Z. and M.F.C. gratefully acknowledge Ryan Klein from the Freedman group at Northwestern University for providing the acetonitrile. L.J. and D.V.C. acknowledge support from the NSF Award CHE-1362825.

■ REFERENCES

(1) Oja, S. M.; Wood, M.; Zhang, B. Nanoscale Electrochemistry. *Anal. Chem.* **2013**, *85*, 473−486.

(2) Oja, S. M.; Fan, Y.; Armstrong, C. M.; Defnet, P.; Zhang, B. Nanoscale Electrochemistry Revisited. *Anal. Chem.* **2016**, *88*, 414−430.

(3) Mathwig, K.; Aartsma, T. J.; Canters, G. W.; Lemay, S. G. Nanoscale Methods for Single-Molecule Electrochemistry. *Annu. Rev. Anal. Chem.* **2014**, *7*, 383−404.

(4) Lei, C.; Hu, D.; Ackerman, E. J. Single-Molecule Fluorescence Spectroelectrochemistry of Cresyl Violet. *Chem. Commun.* **2008**, 5490−5492.

(5) Rao, V. G.; Dhital, B.; He, Y.; Lu, H. P. Single-Molecule Interfacial Electron Transfer Dynamics of Porphyrin on TiO_2 Nanoparticles: Dissecting the Complex Electronic Coupling Dependent Dynamics. *J. Phys. Chem. C* **2014**, *118*, 20209−20221.

(6) Rao, V. G.; Dhital, B.; Lu, H. P. Single-Molecule Interfacial Electron Transfer Dynamics of Porphyrin on TiO_2 Nanoparticles: Dissecting the Interfacial Electric Field and Electron Accepting State Density Dependent Dynamics. *Chem. Commun.* **2015**, *51*, 16821−16824.

(7) Shen, H.; Zhou, X.; Zou, N.; Chen, P. Single-Molecule Kinetics Reveals a Hidden Surface Reaction Intermediate in Single-Nanoparticle Catalysis. *J. Phys. Chem. C* **2014**, *118*, 26902−26911.

(8) Chang, Y.-L.; Palacios, R. E.; Fan, F.-R. F.; Bard, A. J.; Barbara, P. F. Electrogenerated Chemiluminescence of Single Conjugated Polymer Nanoparticles. *J. Am. Chem. Soc.* **2008**, *130*, 8906−8907.

(9) Paxton, W. F.; Kleinman, S. L.; Basuray, A. N.; Stoddart, J. F.; Van Duyne, R. P. Surface-Enhanced Raman Spectroelectrochemistry of TTF-Modified Self-Assembled Monolayers. *J. Phys. Chem. Lett.* **2011**, *2*, 1145−1149.

(10) Cortés, E.; Etchegoin, P. G.; Le Ru, E. C.; Fainstein, A.; Vela, M. E.; Salvarezza, R. C. Monitoring the Electrochemistry of Single Molecules by Surface-Enhanced Raman Spectroscopy. *J. Am. Chem. Soc.* **2010**, *132*, 18034−18037.

(11) Cortés, E.; Etchegoin, P. G.; Le Ru, E. C.; Fainstein, A.; Vela, M. E.; Salvarezza, R. C. Strong Correlation between Molecular Configurations and Charge-Transfer Processes Probed at the Single-Molecule Level by Surface-Enhanced Raman Scattering. *J. Am. Chem. Soc.* **2013**, *135*, 2809−2815.

(12) Wang, Y.; Sevinc, P. C.; He, Y.; Lu, H. P. Probing Ground-State Single-Electron Self-Exchange across a Molecule−Metal Interface. *J. Am. Chem. Soc.* **2011**, *133*, 6989−6996.

(13) Wilson, A. J.; Willets, K. A. Visualizing Site-Specific Redox Potentials on the Surface of Plasmonic Nanoparticle Aggregates with Superlocalization SERS Microscopy. *Nano Lett.* **2014**, *14*, 939−945.

(14) Weber, M. L.; Wilson, A. J.; Willets, K. A. Characterizing the Spatial Dependence of Redox Chemistry on Plasmonic Nanoparticle Electrodes Using Correlated Super-Resolution Surface-Enhanced Raman Scattering Imaging and Electron Microscopy. *J. Phys. Chem. C* **2015**, *119*, 18591−18601.

(15) Kurouski, D.; Mattei, M.; Van Duyne, R. P. Probing Redox Reactions at the Nanoscale with Electrochemical Tip-Enhanced Raman Spectroscopy. *Nano Lett.* **2015**, *15*, 7956−7962.

(16) Tian, Z.-Q.; Ren, B. Adsorption and Reaction at Electrochemical Interfaces as Probed by Surface-Enhanced Raman Spectroscopy. *Annu. Rev. Phys. Chem.* **2004**, *55*, 197−229.

(17) Zong, C.; Chen, C.-J.; Zhang, M.; Wu, D.-Y.; Ren, B. Transient Electrochemical Surface-Enhanced Raman Spectroscopy: A Millisecond Time-Resolved Study of an Electrochemical Redox Process. *J. Am. Chem. Soc.* **2015**, *137*, 11768−11774.

DOI: 10.1021/acs.jpcc.6b09022
J. Phys. Chem. C XXXX, XXX, XXX−XXX

(18) Zaleski, S.; Wilson, A. J.; Mattei, M.; Chen, X.; Goubert, G.; Cardinal, M. F.; Willets, K. A.; Van Duyne, R. P. Investigating Nanoscale Electrochemistry with Surface- and Tip-Enhanced Raman Spectroscopy. *Acc. Chem. Res.* **2016**, *49*, 2023−2030.
(19) Ni, F.; Feng, H.; Gorton, L.; Cotton, T. M. Electrochemical and Sers Studies of Chemically Modified Electrodes: Nile Blue A, a Mediator for NADH Oxidation. *Langmuir* **1990**, *6*, 66−73.
(20) Wilson, A. J.; Willets, K. A. Unforeseen Distance-Dependent SERS Spectroelectrochemistry from Surface-Tethered Nile Blue: The Role of Molecular Orientation. *Analyst* **2016**, *141*, 5144−5151.
(21) Wilson, A. J.; Molina, N. Y.; Willets, K. A. Modification of the Electrochemical Properties of Nile Blue through Covalent Attachment to Gold as Revealed by Electrochemistry and SERS. *J. Phys. Chem. C* **2016**, *120*, 21091−21098.
(22) Zaleski, S.; Cardinal, M. F.; Klingsporn, J. M.; Van Duyne, R. P. Observing Single, Heterogeneous, One-Electron Transfer Reactions. *J. Phys. Chem. C* **2015**, *119*, 28226−28234.
(23) Jäckel, F.; Kinkhabwala, A. A.; Moerner, W. E. Gold Bowtie Nanoantennas for Surface-Enhanced Raman Scattering under Controlled Electrochemical Potential. *Chem. Phys. Lett.* **2007**, *446*, 339−343.
(24) Shegai, T.; Vaskevich, A.; Rubinstein, I.; Haran, G. Raman Spectroelectrochemistry of Molecules within Individual Electromagnetic Hot Spots. *J. Am. Chem. Soc.* **2009**, *131*, 14390−14398.
(25) Hermanson, G. *Zero-Length Crosslinkers in Bioconjugate Techniques*; Academic Press: Boston, 2013.
(26) Lee, P. C.; Meisel, D. Adsorption and Surface-Enhanced Raman of Dyes on Silver and Gold Sols. *J. Phys. Chem.* **1982**, *86*, 3391−3395.
(27) Valiev, M.; et al. Nwchem: A Comprehensive and Scalable Open-Source Solution for Large Scale Molecular Simulations. *Comput. Phys. Commun.* **2010**, *181*, 1477−1489.
(28) Sonntag, M. D.; Klingsporn, J. M.; Garibay, L. K.; Roberts, J. M.; Dieringer, J. A.; Seideman, T.; Scheidt, K. A.; Jensen, L.; Schatz, G. C.; Van Duyne, R. P. Single-Molecule Tip-Enhanced Raman Spectroscopy. *J. Phys. Chem. C* **2012**, *116*, 478−483.
(29) Kubin, R. F.; Fletcher, A. N. Fluorescence Quantum Yields of Some Rhodamine Dyes. *J. Lumin.* **1982**, *27*, 455−462.
(30) van de Linde, S.; Krstic, I.; Prisner, T.; Doose, S.; Heilemann, M.; Sauer, M. Photoinduced Formation of Reversible Dye Radicals and Their Impact on Super-Resolution Imaging. *Photochem. & Photobiol. Sci.* **2011**, *10*, 499−506.
(31) Klingsporn, J. M.; Jiang, N.; Pozzi, E. A.; Sonntag, M. D.; Chulhai, D.; Seideman, T.; Jensen, L.; Hersam, M. C.; Duyne, R. P. V. Intramolecular Insight into Adsorbate−Substrate Interactions Via Low-Temperature, Ultrahigh-Vacuum Tip-Enhanced Raman Spectroscopy. *J. Am. Chem. Soc.* **2014**, *136*, 3881−3887.
(32) Laviron, E. Adsorption, Autoinhibition and Autocatalysis in Polarography and in Linear Potential Sweep Voltammetry. *J. Electroanal. Chem. Interfacial Electrochem.* **1974**, *52*, 355−393.
(33) Brown, A. P.; Anson, F. C. Cyclic and Differential Pulse Voltammetric Behavior of Reactants Confined to the Electrode Surface. *Anal. Chem.* **1977**, *49*, 1589−1595.
(34) Bard, A. J.; Faulkner, L. R. *Electrochemical Methods: Fundamentals and Applications*, 2nd ed.; Wiley: New York, 2000.
(35) Chidsey, C. E. D.; Bertozzi, C. R.; Putvinski, T. M.; Mujsce, A. M. Coadsorption of Ferrocene-Terminated and Unsubstituted Alkanethiols on Gold: Electroactive Self-Assembled Monolayers. *J. Am. Chem. Soc.* **1990**, *112*, 4301−4306.
(36) Greeneltch, N. G.; Blaber, M. G.; Henry, A.-I.; Schatz, G. C.; Van Duyne, R. P. Immobilized Nanorod Assemblies: Fabrication and Understanding of Large Area Surface-Enhanced Raman Spectroscopy Substrates. *Anal. Chem.* **2013**, *85*, 2297−2303.
(37) Sharma, B.; Fernanda Cardinal, M.; Kleinman, S. L.; Greeneltch, N. G.; Frontiera, R. R.; Blaber, M. G.; Schatz, G. C.; Van Duyne, R. P. High-Performance SERS Substrates: Advances and Challenges. *MRS Bull.* **2013**, *38*, 615−624.
(38) Le Ru, E. C.; Etchegoin, P. G. *Principles of Surface-Enhanced Raman Spectroscopy*; Elsevier: Amsterdam, 2009.
(39) Wolkow, R. A.; Moskovits, M. Enhanced Photochemistry on Silver Surfaces. *J. Chem. Phys.* **1987**, *87*, 5858−5869.
(40) Etchegoin, P. G.; Le Ru, E. C. Resolving Single Molecules in Surface-Enhanced Raman Scattering within the Inhomogeneous Broadening of Raman Peaks. *Anal. Chem.* **2010**, *82*, 2888−2892.

DOI: 10.1021/acs.jpcc.6b09022
J. Phys. Chem. C XXXX, XXX, XXX−XXX